Influence of the Preparation Methods on the Microstructure and Oxygen Permeability of a CO_2-Stable Dual Phase Membrane

Huixia Luo, Heqing Jiang, Konstantin Efimov, and Jürgen Caro
Institute of Physical Chemistry and Electrochemistry, Leibniz University of Hannover, D-30167 Hannover, Germany

Haihui Wang
School of Chemistry and Chemical Engineering, South China University of Technology, Guangzhou 510640, China

DOI 10.1002/aic.12488
Published online December 17, 2010 in Wiley Online Library (wileyonlinelibrary.com).

A CO_2-stable dual phase membrane of the composition 40 wt % $NiFe_2O_4$-60 wt % $Ce_{0.9}Gd_{0.1}O_{2-\delta}$ (40NFO-60CGO) was synthesized in three different ways: mixing of the starting powders (1) in a mortar and (2) in a ball-mill as well as by (3) direct in situ *one-pot sol–gel powder synthesis. Backscattered scanning electron microscopy revealed that the direct one-pot synthesis of 40NFO-60CGO gives the smallest grains in a homogeneous distribution, compared with powder homogenization in the mortar or the ball-mill. The smaller is the grains, the higher is the oxygen permeability. The permeation of the membrane can be improved by coating a porous $La_{0.6}Sr_{0.4}CoO_{3-\delta}$ (LSC) layer on the surface of the air side. The dual phase membrane of 40NFO-60CGO prepared by* in situ *synthesis shows a steady oxygen flux of 0.30 ml/(min cm^2) over more than 100 h when pure CO_2 was used as sweep gas, which indicated that the dual phases membrane is CO_2-resistant at least over this 5 days testing period.* © 2010 American Institute of Chemical Engineers *AIChE J,* 57: 2738–2745, 2011
Keywords: homogeneity, dual phase membrane, oxygen separation, CO_2-stable

Introduction

The increasing carbon dioxide emission, especially from power generation industry, is considered as the main source of global warming.[1] To minimize the impact of the CO_2 emission on the climate change, great efforts are devoted to recover and sequestrate CO_2.[2–4] One potential route is the oxy-fuel concept burning natural gas with nitrogen-free oxygen, which allows to sequestrate the CO_2 after steam condensation. Dense mixed oxygen ionic-electronic conducting ceramic membranes (MIECM), perovskites are promising candidates for this oxygen separation from air.[5–14] However, when MIECMs are used for the separation of oxygen from air, some of the CO_2 is recycled and used as the sweep gas for the oxygen separation, simultaneously lowering the temperature in the burner.[15–17]

A handicap of most of the perovskite materials for their application in the oxy-fuel technology is their instability in the presence of CO_2 because of the carbonate formation because the perovskite type membranes usually contain alkaline earth ions like Ba^{2+} or Sr^{2+} on the A-site, which tend to react with CO_2 and form carbonates.[18,19] An alternative is the development of composite membranes of two separate CO_2-stable electron and oxygen-ion conducting phases. Up to now, numerous dual phase materials have been developed which can be divided into two major groups: (1) The first generation of dual phase membranes were composites of noble metal powders as electronic and a ceramic particles as ionic conductors.[20–22] However, these composite membranes are expensive, a mismatch of the thermal expansion

Correspondence concerning this article should be addressed to J. Caro at juergen.caro@pci.uni-hannover.de (or) H. Wang at hhwang@scut.edu.cn.

© 2010 American Institute of Chemical Engineers

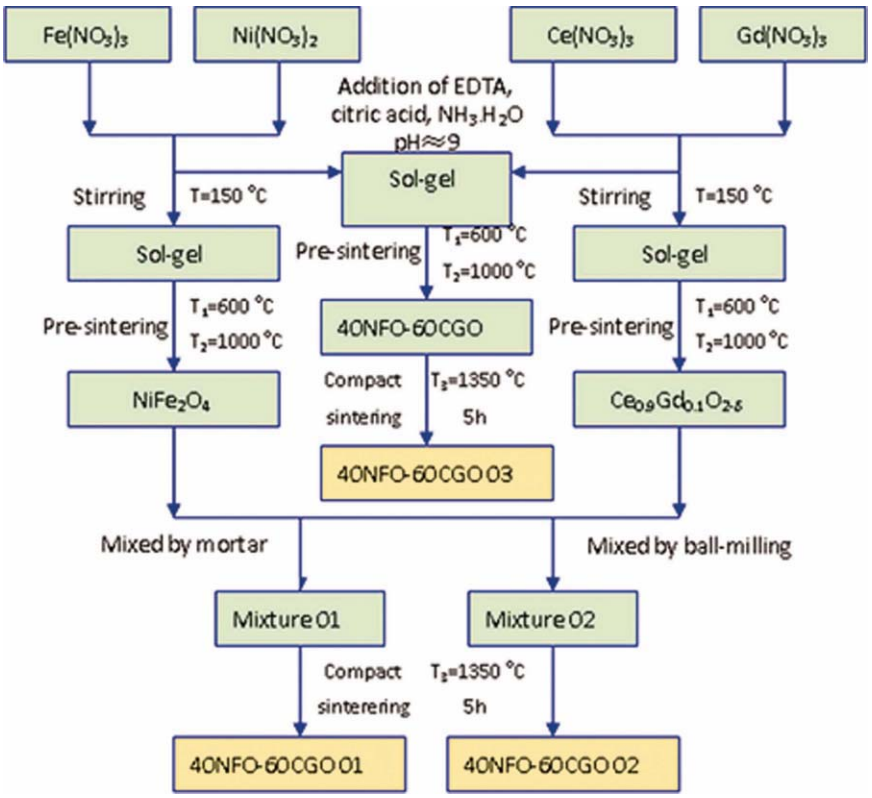

Figure 1. Flowchart for the preparation of dual phase membranes.

[Color figure can be viewed in the online issue, which is available at wileyonlinelibrary.com.]

coefficients (TEC) of the metallic and the ceramic phase exists, and the oxygen permeabilities were found to be low. (2) The second generation of dual phase membranes were composites of two oxides, where one of the oxides acts as electron conductor instead of the noble metal.[23–25] These dual phase membranes of the second generation show higher oxygen permeabilities, but they usually contain a perovskite phase (ABO_3, A = alkalin earth metals or lanthanide element; B = transition metal). The alkaline earth metals on the A site easily form carbonates if CO_2 is present. This carbonate formation is found to be reversible but it immediately stops the oxygen flux.[18,19] These dual phase membranes also suffer from a mechanical stress and can mechanically decompose due to swelling by carbonate formation.

In this article, a novel earth alkaline metal-free CO_2-stable dual phase membrane has been developed. The $NiFe_2O_4$ (NFO) and $Ce_{0.9}Gd_{0.1}O_{2-\delta}$ (CGO) powders have been mixed in a mortar and a ball-mill, and the NFO-CGO dual phase was also obtained directly in an *in situ* one-pot sol–gel synthesis. The chemical composition of our dual phase membrane is 40 wt % $NiFe_2O_4$-60 wt % $Ce_{0.9}Gd_{0.1}O_{2-\delta}$ (40NFO-60CGO). In the mixture of the two phases, NFO is the electron conductor and CGO is the oxygen ion conductor. The microstructure of the membranes will be correlated with the oxygen permeability.

Experimental Section

The powders of CGO, NFO, and 40 wt % $NiFe_2O_4$-60 wt % $Ce_{0.9}Gd_{0.1}O_{2-\delta}$ were synthesized by a combined citrate and EDTA complexing method. After stirring the metal nitrate solutions for 20 min, calculated amounts of citrate and EDTA were added and the pH value was adjusted to ~9 by ammonia. The molar ratio of EDTA:citric acid:total metal ions was 1:1.5:1. Then, the solutions were stirred when heated to 150°C, until the water was evaporated and a gel was formed. The gels were calcined in air at 600°C in a furnace to remove the organic compounds by combustion, and the primary powders were obtained. These powders were calcined at 1000°C for 10 h.

The 40NFO-60CGO dual phase membranes were prepared in three ways. Figure 1 shows the three methods applied in this article for the dual phase preparation. (1) Powder mixing in a mortar (membrane 40NFO-60CGO 01): The as-obtained CGO and NFO powders were mixed with a weight ratio of 60:40. Then, the mixed powders were ground in an agate mortar for 1.5 h. (2) Powder mixing by ball-milling (membrane 40NFO-60CGO 02): The as-obtained CGO and NFO powders were mixed in a weight ratio 60:40 by ball-milling for 4 h. (3) Direct one-pot sol–gel synthesis (membrane 40NFO-60CGO 03): The powder mixture was obtained *in situ*.

The powders of all three techniques were pressed to disk membranes under a pressure of ~10 MPa in a stainless steel module with a diameter of 16 mm. Then, they were sintered at 1350°C in air for 10 h with heating and cooling rates of 2°C/min. The membranes were polished to 0.6 mm thickness by using 1200 grit-sand paper (average particle diameter 15.3 μm), then the membranes were washed with ethanol. To improve the oxygen surface exchange rate on the air

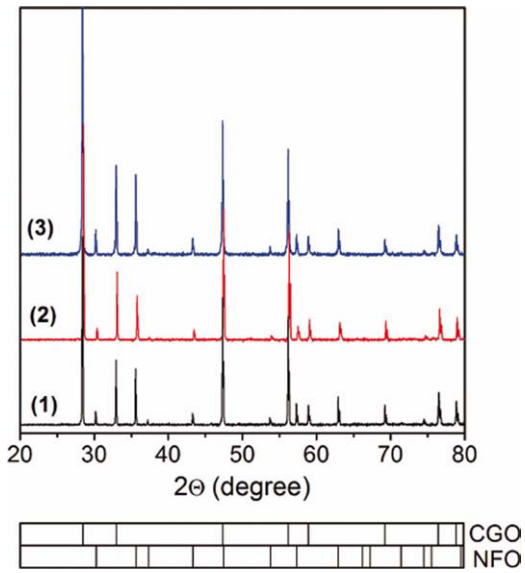

Figure 2. XRD patterns of 40NFO-60CGO membranes prepared by different methods.

Mixing of the NFO and CGO powder (1) in an agate mortar and (2) by ball-milling. (3) Direct synthesis of the powder in a one-pot synthesis. The theoretical Bragg position for CGO (PDF 46-507) and NFO (PDF 10-325) are labeled with the ticks at the bottom of the figure. [Color figure can be viewed in the online issue, which is available at wileyonlinelibrary.com.]

side, a $La_{0.6}Sr_{0.4}CoO_{3-\delta}$ (LSC) porous layer[26,27] was deposited with a paste made of 40 wt % LSC powder and 60 wt % terpineol. After coating the membrane with LSC, the composite was calcined at 950°C for 2 h.

The phase structure of the dual phase membranes were studied by X-ray diffraction (XRD, D8 Advance, Bruker-AXS, with Cu Kα radiation) after grinding the membranes to a size of 10–100 μm. Data sets were recorded in a step–scan mode in the 2Θ range of 20–80° with intervals of 0.02°. *In situ* XRD tests were conducted in a high-temperature cell HTK-1200N (Anton-Paar) between room temperature and 1000°C. For tests in ambient air, heating and cooling rate were set to 6°C/min. Before each data acquisition, an equilibration time of 70 min was used. Tests in the atmosphere containing 50 vol % CO_2/50 vol % N_2 were carried out with heating and cooling rate of 12°C/min. At each temperature step, the temperature was held for 30 min before diffraction data collection. The surface and cross section morphology of the membrane disks were studied by scanning electron microscopy (SEM) using the Jeol-JSM-6700F. Some micrographs were taken in the back scattering mode (BSEM).

Oxygen permeation was studied in a self-made high-temperature oxygen permeation cell, described in Ref. 28. A gold paste (Heraeus) was used to seal the disk onto a quartz tube at 950°C for 5 h. As feed a 50 vol % O_2/50 vol % N_2 mixed gas was used; as sweep gases He and CO_2 have been used (29 ml/min, 99.995% + 1 ml Ne/min as an internal standard gas). A gas chromatograph (GC, Agilent 6890) was connected to the effluents of the sweep side. The GC was frequently calibrated using standard gases to ensure the reliability of the experimental data. The leakage is caused by the imperfect sealing at high temperature, which can be determined by the detecting N_2 by GC. In no case, the leakage stream is larger than 5% of the oxygen flux through the membrane. Assuming that leakage of nitrogen and oxygen is in accordance with Knudsen diffusion, the fluxes of leaked N_2 and O_2 are related by

$$J_{N_2}^{Leak} : J_{O_2}^{Leak} = \sqrt{\frac{32}{28}} \times \frac{0.79}{0.21} = 4.02.$$

The oxygen permeation flux was then calculated as follows:

$$J_{O_2}[\mathrm{ml}/(\mathrm{min\ cm}^2)] = \left(C_{O_2} - \frac{C_{N_2}}{4.02}\right) \times \frac{F}{S}$$

where C_{O_2} and C_{N_2} are the oxygen and nitrogen concentrations, respectively, calculated from GC calibration, F is the total flow rate of the outlet on the sweep side, which was measured by the change of Ne concentration before and after permeator.

The total flow rate of the effluents was calculated from the change in the Ne concentrations before and after the permeator.

Results and Discussion

Characteristics of the dual phase materials

Figure 2 shows the XRD patterns of the 40NFO-60CGO membranes prepared by three different methods, by powder mixing (1) in a mortar and (2) in a ball-milling as well as (3) the direct synthesis of the mixed powders by a one-pot method. All the composite membranes consist of only the two phases, NFO and CGO, and no other crystalline phases have been formed. From the similarity of the lattice parameters of the NFO and CGO phases as shown in Table 1, a good phase compatibility in the mixed material can be expected.

The influence of the different preparation methods on the microstructure of 40NFO-60CGO dual phase membranes is shown in Figure 3. When comparing the SEM and BSEM pictures, we can see clear differences of the size and uniformity of the NFO and CGO grains as well as of their homogeneous distribution of the three membranes under study. Membrane 40NFO-60CGO 03 made by *in situ* direct sol–gel synthesis has the smallest grain size (0.2–1.5 μm) but—as shown later—the highest oxygen permeation flux. On the contrary, 40NFO-60CGO 01 made by powder mixing in a mortar has the largest grains and lowest oxygen permeation flux. Furthermore, in this membrane, the NFO grains are bigger (3–7 μm) than the CGO grains (2–4 μm). Grain size of 40NFO-60CGO 02 made by ball-milling is in the range 0.4–2 μm, which is between the grain sizes of 40NFO-60CGO

Table 1. Lattice Parameters of NFO and CGO as Pure Phases and in the 40NFO-60CGO Dual Phase Membranes Prepared by Different Methods

Phase	Pure Phase	40NFO-60CGO 01 Mortar	40NFO-60CGO 02 Ball-Milling	40NFO-60CGO 03 One-Pot Method
NFO (Å)	8.3455	8.3641	8.3195	8.3596
CGO (Å)	5.4209	5.4400	5.4106	5.4326

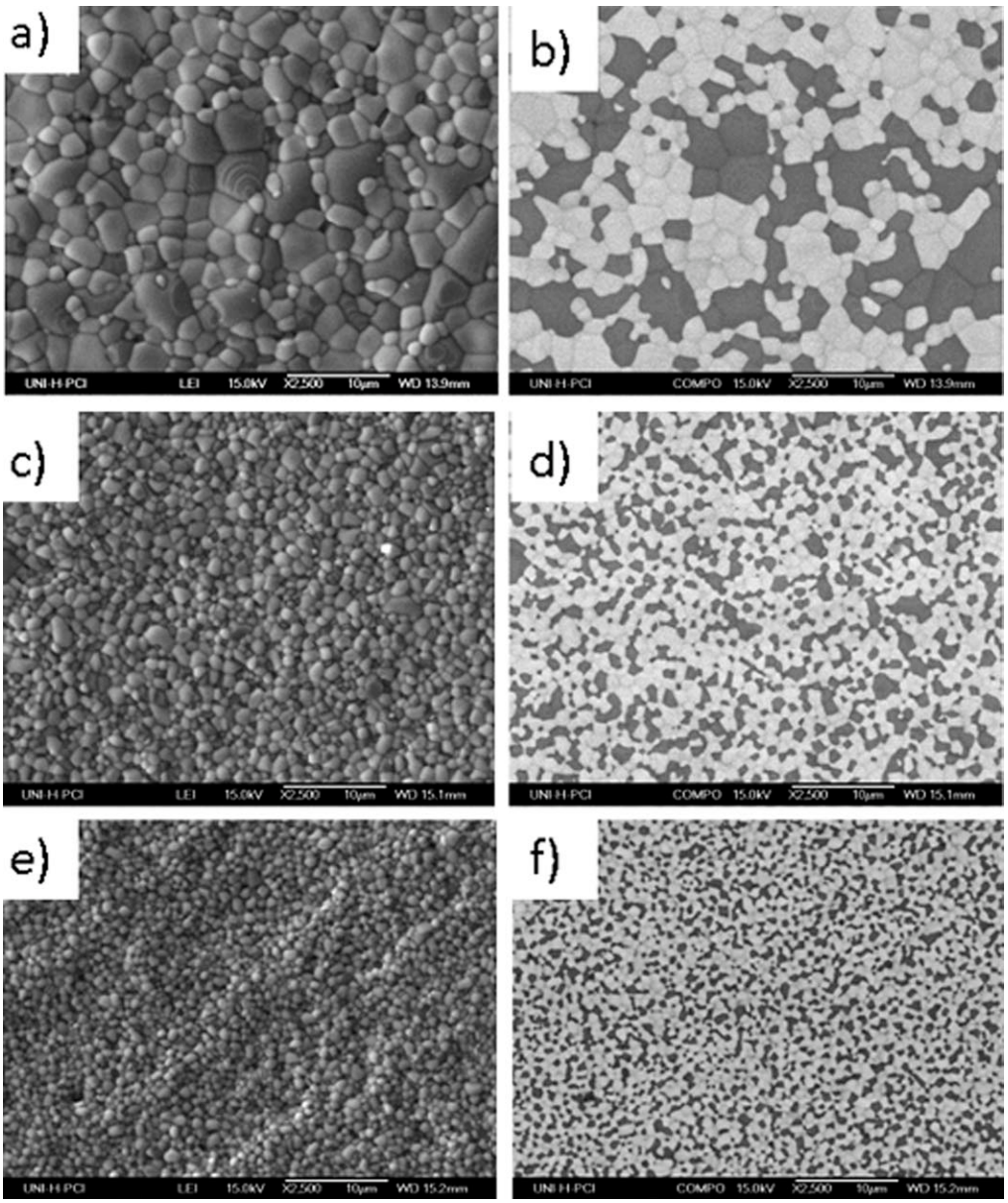

Figure 3. SEM (left column) and BSEM (right column) of the surface grain structure of the membranes 40NFO-60CGO 01, 02, and 03, prepared by powder mixing in a mortar (a and b), ball-milling (c and d), and one-pot method (e and f), respectively.

01 and 40NFO-60CGO 03, and consequently, the oxygen permeation flux is in between.

Structure stability and thermal expansion coefficient of the dual phase materials 40NFO-60CGO

In situ XRD provides an effective and direct way to characterize the high-temperature structure changes during increasing and decreasing temperatures under certain gas atmospheres. Figures 4 and 5 show the XRD patterns of the NFO and CGO powders in air for increasing and decreasing temperatures between 30°C and 1000°C indicating that the phases CGO and NFO remain unchanged.

Figure 6 shows the lattice constants of NFO and CGO at various temperatures determined from the *in situ* XRD data in air. As expected, the lattice constants depend linearly on temperatures for both NFO and CGO with increasing and decreasing temperatures. The TEC was calculated following the definition $\frac{d(\Delta a/a_0)}{dT}$ (a is the lattice constant and a_0 is the lattice constant at room temperature). The values of the TEC of NFO and CGO calculated from the data of Figure 6 for the range of 30–1000°C. The TEC of NFO ($4.36 \pm 0.3 \times 10^{-5}$ K^{-1}) is higher than that of CGO ($1.81 \pm 0.1 \times 10^{-5}$ K^{-1}). However, when the membrane was sintered, because of the different TECs of the two phases, the heating and cooling rate should not be faster than 2°C/min to avoid cracking of the membranes.

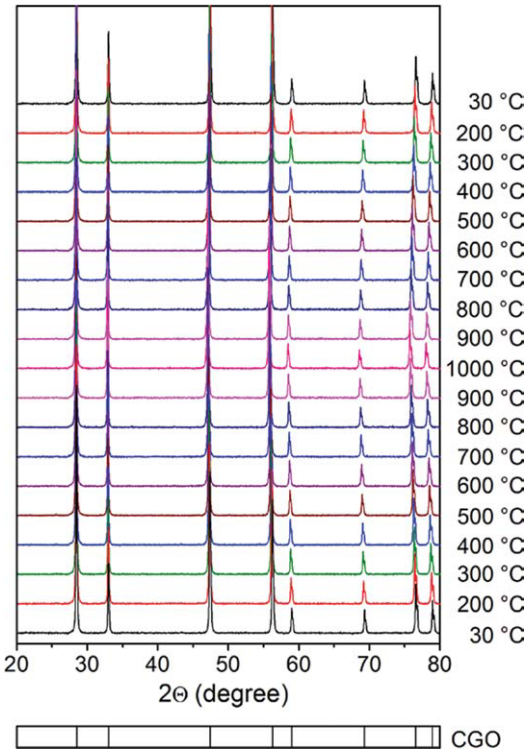

Figure 4. *In situ* XRD patterns of CGO under air during increasing and decreasing temperatures.

Heating and cooling rates = 6°C/min, equilibration time at each temperature: 70 min for recording the XRD. [Color figure can be viewed in the online issue, which is available at wileyonlinelibrary.com.]

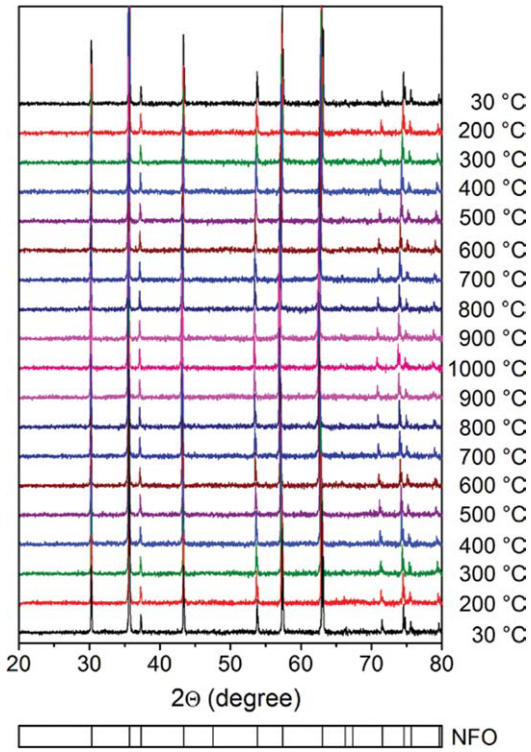

Figure 5. *In situ* XRD patterns of NFO under air during increasing and decreasing temperatures.

Heating and cooling rates = 6°C/min, equilibration time at each temperature: 70 min for recording the XRD. [Color figure can be viewed in the online issue, which is available at wileyonlinelibrary.com.]

For a potential application of MIECM membranes in the oxy-fuel technology, the membranes must be stable in a carbon dioxide atmosphere. Therefore, the high-temperature phase stability of 40NFO-60CGO 03 in the CO_2 containing atmosphere of 50 vol % CO_2/50 vol % air has been studied by *in situ* XRD, as shown in Figure 7. The two phases NFO and CGO remained unchanged, no carbonates were found.

Influence of grain size on the oxygen permeability of dual phase membrane

Figure 8 shows the oxygen permeation of the three 40NFO-60CGO membranes under study at 950°C. It can be found that the oxygen permeation fluxes of membrane 40NFO-60CGO 01 decreases with increasing permeation time at the initial stage. After around 1200 min, the permeation oxygen fluxes of 40NFO-60CGO 01 reach a steady state. However, the oxygen permeation fluxes through both membrane 40NFO-60CGO 02 and membrane 40NFO-60CGO 03 increase with permeation time at the initial stage and then they reach a steady state. The steady-state oxygen permeances of our 40NFO-60CGO membranes are 01 < 02 < 03, which correlate clearly with the size of the NFO and CGO grains in the mixed matrix. A similar decline of oxygen permeation flux through the dual-phase composite membranes with time has been reported in a previous paper.[27] However, the detailed reason for this time-dependent behavior is not clear.[29] It follows from Figure 8 that the steady oxygen permeation flux through 40NFO-60CGO 03 is the highest among the three type of membranes. According to the previous studies,[27,30] the oxygen permeation flux is determined not only by the conductivities of both phases but also by the grain sizes as well as grain size distribution, which can be described by the percolation theory. BSEM results (cf. Figure 3) revealed that the direct one-pot synthesis of 40NFO-60CGO 03 gives the smallest grains in a

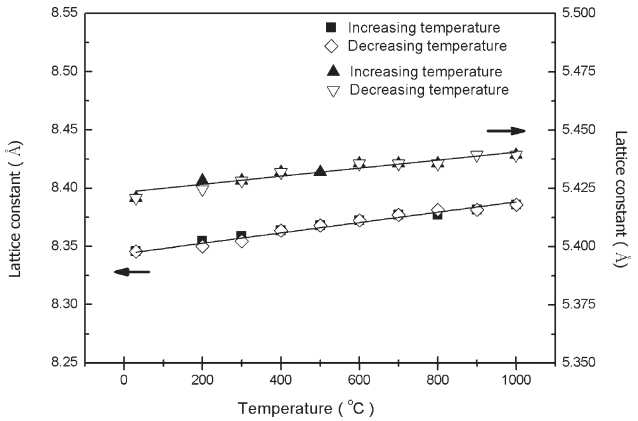

Figure 6. Temperature dependence of the lattice constants for NFO (■ increasing temperature, ◇ decreasing temperature) and CGO (▲ increasing temperature, ▽ decreasing temperature).

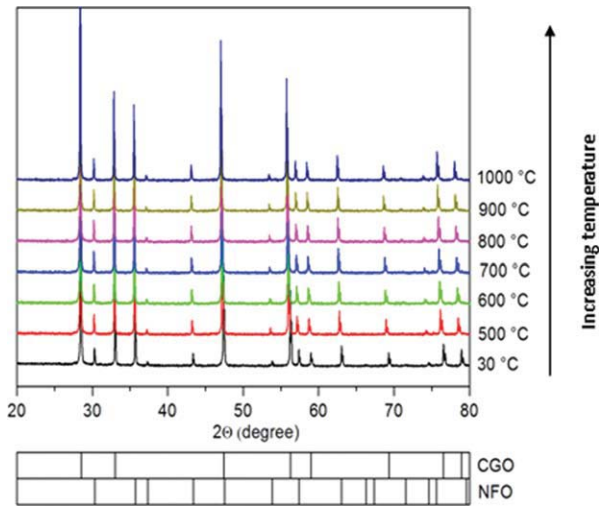

Figure 7. *In situ* XRD patterns of the one-pot 40NFO-60CGO 03 powder under 50% CO_2/50% air at different temperatures.

Heating rates = 12°C/min, equilibration time at each temperature: 30 min for recording the XRD. [Color figure can be viewed in the online issue, which is available at wileyonlinelibrary.com.]

homogeneous distribution, so a highest of oxygen permeation flux was obtained compared with powder homogenization in the mortar or the ball-mill.

Figure 9 shows the oxygen permeability of the three 40NFO-60CGO dual phase membranes as a function of temperature. The data were obtained after the permeation having reached steady state. In agreement with the results shown in Figure 8, in the temperature window between 900°C and 1000°C, the dual phase membrane 03 prepared by the direct *in situ* sol–gel method with the smallest grains shows the highest oxygen permeation fluxes followed by the membrane 02 made by ball-milling with medium grain size and finally by the membrane 01 with the highest grain size made by powder mixing. The Arrhenius plots of the oxygen permeation fluxes through composite membranes (Figure 10) show that the permeation activation energy of membrane 03 E_a = 67.48 kJ/mol is the smallest of the three membranes, whereas the E_a of membranes 02 and 03 are ~112.0 and ~107.9 kJ/mol, respectively. Similar results were reported in 75 wt % $Ce_{0.8}Gd_{0.2}O_{1.9}$-25 wt % $Gd_{0.2}Sr_{0.8}FeO_{3-\delta}$ (GDC-GSF) dual phase membranes.[27]

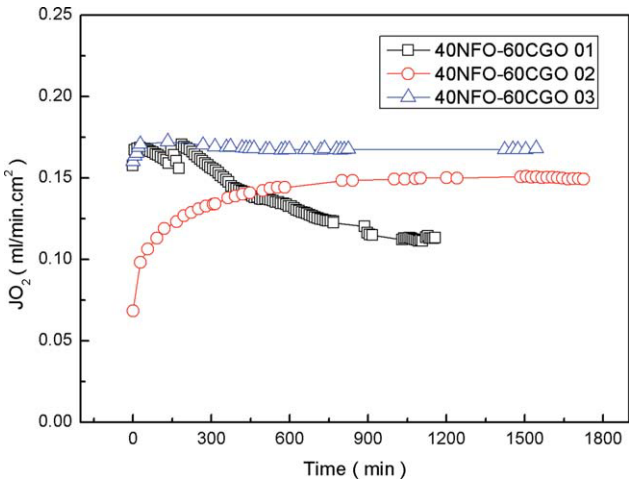

Figure 8. Oxygen permeation flux through 40NFO-60CGO composite membranes without coating as a function of time at 950°C.

Feed: 150 ml/min 50 vol % O_2 with 50 vol % N_2. Sweep: 29 ml/min He + 1 ml/min Ne as internal standard gas, thickness of membranes = 0.6 mm. [Color figure can be viewed in the online issue, which is available at wileyonlinelibrary.com.]

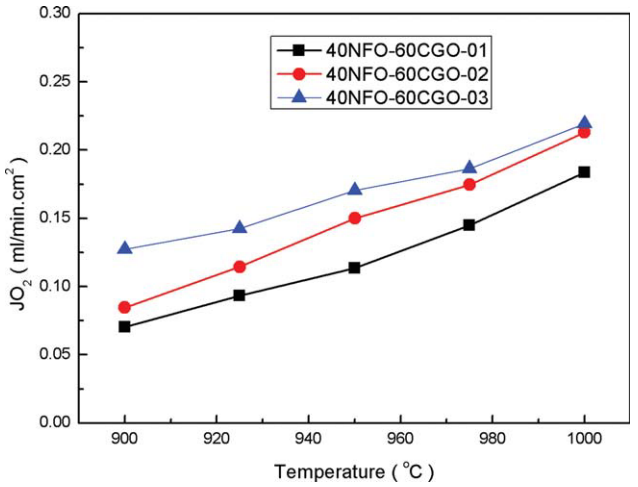

Figure 9. Temperature dependence of the oxygen permeation fluxes through 40NFO-60CGO membranes prepared by different methods without coating.

Feed: 150 ml/min 50 vol % O_2 with 50 vol % N_2. Sweep: 29 ml/min He + 1 ml/min Ne as internal standard gas. Thickness of membranes = 0.6 mm. [Color figure can be viewed in the online issue, which is available at wileyonlinelibrary.com.]

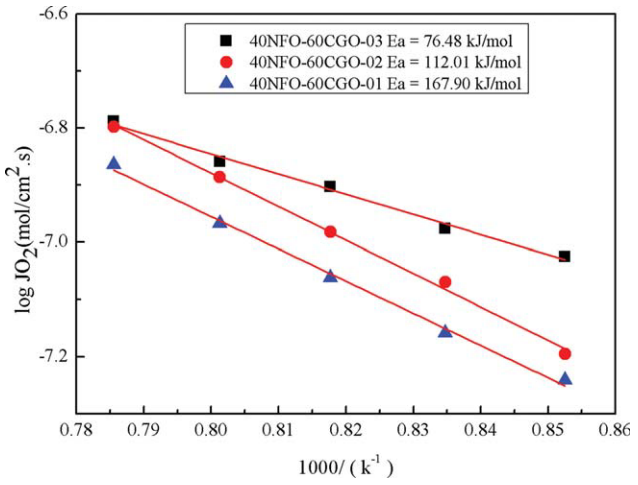

Figure 10. Arrhenius plots of the oxygen permeation fluxes through 40NFO-60CGO dual phase membranes (for the experimental conditions see Figure 9).

[Color figure can be viewed in the online issue, which is available at wileyonlinelibrary.com.]

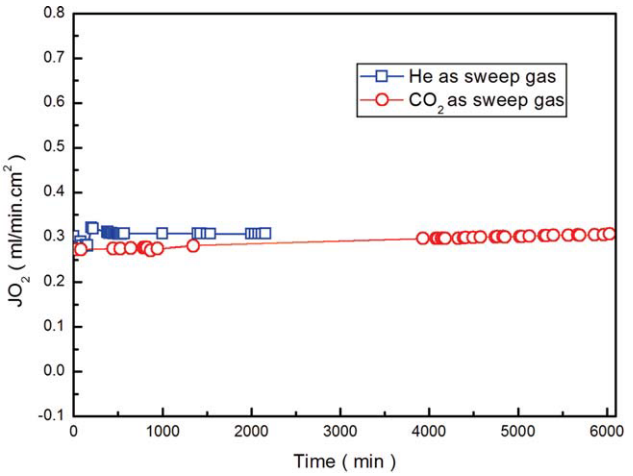

Figure 11. Oxygen permeation flux of the 40NFO-60CGO 03 composite membrane with LSC coating as a function of time at 1000°C, membrane thickness = 0.6 mm.

Feed: 150 ml/min synthetic air with 20 vol % O_2. Sweep: 29 ml/min He + 1 ml/min Ne as an internal standard gas. [Color figure can be viewed in the online issue, which is available at wileyonlinelibrary.com.]

CO_2-stability of 40NFO-60CGO 03 membrane

Because membrane 40NFO-60CGO 03 made by the direct *in situ* sol–gel synthesis showed the highest oxygen permeation flux, we selected this membrane for CO_2 stability tests and for further surface modification. To improve the oxygen surface exchange rate on the air side, the 40NFO-60CGO 03 membrane was coated with $La_{0.6}Sr_{0.4}CoO_{3-\delta}$ (LSC) porous layer on one side using a paste made of 40 wt % LSC powder and 60 wt % terpineol. The low CO_2 partial pressure in natural air will not cause a strontium carbonate formation above 722°C.[31] In our experiments, however, synthetic air was used. After coating with the LSC layer, the membrane 40NFO-60CGO 03 was calcined at 950°C for 2 h in air to burn the organics.

Figure 11 shows the dependence of the oxygen permeation flux of the 40NFO-60CGO 03 composite membrane as a function on time at 1000°C with pure He or CO_2 as sweep gases. From Figure 11, we can find that the LSC coated membrane 03 reaches steady-state oxygen permeation like the uncoated membrane 03 after a relative short time in comparison with the uncoated membranes 01 and 02 (cf. Figure 8). There is almost no difference between using He or CO_2 as sweep gases, which indicates that the membrane 40NFO-60CGO 03 membrane is really CO_2 tolerant. Furthermore, the membrane was operated for 100 h in the oxygen separation with pure CO_2 as the sweep gas which again indicates that the material composition 40NFO-60CGO was found to be CO_2-stable—at least for our 5 days of testing which is a relative short time scale from an industrial point of view. However, the oxygen permeation flux is found to be slightly lower when CO_2 is used as sweep gas in comparison with He. This difference can be explained by the inhibiting effect of carbon dioxide on the oxygen surface exchange reaction, i.e., the presence of CO_2 reduces the rate of the oxygen release from the solid. This assumption is in complete agreement with previous papers,[32–34] which report that the oxygen surface exchange reaction is not the same in different gas atmospheres.

Conclusions

Different synthesis methods for the preparation of a carbon dioxide resistant dual phase membrane of the composition 40 wt % $NiFe_2O_4$-60 wt % $Ce_{0.9}Gd_{0.1}O_{2-\delta}$ (40NFO-60CGO) with NFO as electron conductor and CGO as oxygen ion conductor have been evaluated. The membrane prepared by a direct one-pot synthesis shows the smallest grains and the highest oxygen permeation fluxes in the range 900–1000°C. On the opposite, the membranes prepared by mixing the NFO and CGO powders in a mortar or by ball-milling give larger grains and a lower oxygen permeation flux. High-temperature XRD in CO_2 containing atmospheres showed that the NFO and CGO phases in 40NFO-60CGO 03 remained unchanged, and no carbonate was formed. In long-time permeation studies with CO_2 as sweep gas, we also found that the dual phase membrane 40NFO-60CGO 03 was CO_2 stable and an average oxygen flux of 0.30 ml/(min cm^2) was obtained at 1000°C for a 0.5-mm-thick membrane. This value is comparable with them of $La_2NiO_{4+\delta}$ as well as $La_2Ni_{0.9}Fe_{0.1}O_{4+\delta}$, which are promising CO_2-stable membrane materials.[35]

Acknowledgments

The author (H.X. Luo) acknowledges the financial support by the China Scholarship Council (CSC). K. Efimov thanks the State of Lower Saxony for the NTH bottom up grant No. 21-71023-25-7/09. H.H. Wang greatly acknowledges the financial support by the National Natural Science Foundation of China (nos. 20706020 and U0834004), the National Basic Research Program of China (no. 2009CB623406), and the International Joint Project of Guangdong Province Science and Technology (2009B050700017). The authors also greatly acknowledge Dr. A. Feldhoff for stimulating discussions as well as F. Steinbach and F.Y. Liang for technical support.

Literature Cited

1. Herzog H, Golomb D, Zemba, S. Feasibility, modeling and economics of sequesteing power plant CO_2 emission in the deep ocean. *Environ Prog*. 2006;10:64–74.
2. Lozza G, Chiesa P. Natural gas decarbonization to reduce CO_2 emission from combined cycles. I. Partial oxidation. *ASME J Eng Gas Turbines Power*. 2002;124:82–88.
3. Corradetti A, Desideri U. Analysis of gas-steam combined cycles with natural gas reforming and CO_2 capture. *ASME J Eng Gas Turbines Power*. 2005;127:545–552.
4. Chiesa P, Consonni S. Natural gas fired combined cycles with low CO_2 emission. *ASME J Eng Gas Turbines Power*. 2000;122:429–436.
5. Luo HX, Wei YY, Jiang HQ, Yuan, WH, Lv YX, Caro J, Wang HH. Performance of a ceramic membrane reactor with high oxygen flux Ta-containing perovskite for the partial oxidation of methane to syngas. *J Membr Sci*. 2010;350:154–160.
6. Jiang HQ, Wang HH, Werth S, Schiestel T, Caro J. Simultaneous production of hydrogen and synthesis gas by combining water splitting with partial oxidation of methane in a hollow fiber membrane reactor. *Angew Chem Int Ed Engl*. 2008;47:9341–9344.
7. Jiang HQ, Cao ZW, Schirrmeister S, Schiestel T, Caro J. A coupling strategy to produce hydrogen and ethylene in a membrane reactor. *Angew Chem Int Ed Engl*. 2010;49:5656–5660.
8. Jiang HQ, Liang FY, Czuprat O, Efimov K, Feldhoff A, Schirrmeister S, Schiestel T, Wang HH, Caro J. Hydrogen production by water dissociation in surface-modified $BaCo_xFe_yZr_{1-x-y}O_{3-\delta}$ hollow fiber membrane reactor with improved oxygen permeation. *Chem Eur J*. 2010;16:7898–7903.

9. Jiang HQ, Wang HH, Liang FY, Werth S, Schiestel T, Caro J. Direct decomposition of nitrous oxide to nitrogen by in situ oxygen removal with a perovskite membrane. *Angew Chem Int Ed Engl*. 2009;48:2983–2986.
10. Chen CS, Feng SJ, Ran S, Zhu DC, Liu W, Bouwmeester HJM. Conversion of methane to syngas by a membrane-based oxidation-reforming process. *Angew Chem Int Ed Engl*. 2003;42:5196–5198.
11. Jin WQ, Zhang C, Zhang P, Fan YQ, Xu NP. Thermal decomposition of carbon dioxide coupled with POM in a membrane reactor. *AIChE J*. 2006;52:2545–2550.
12. Tsai CY, Dixon AG, Moser WR, Ma YH. Dense perovskite membrane reactor for partial oxidation of methane to syngas. *AIChE J*. 1997;43:2741–2750.
13. Smart S, Lin CXC, Ding L, Thambimuthu K, Diniz da Costa JC. Ceramic membranes for gas processing in coal gasification. *Energy Environ Sci*. 2010;3:268–278.
14. Tan XY, Li K, Thursfield A, Metcalfe IS. Oxyfuel combustion using a catalytic ceramic membrane reactor. *Catal Today*. 2008;131:292–304.
15. Zhang N, Lior N. Two novel-fuel power cycles integrated with natural gas reforming and CO_2 capture. *Energy*. 2008;33:340–351.
16. Plasynski SI, Litynski JT, Mcllvried HG, Srivastava RD. Progress and new developments in carbon capture. *Crit Rev Plant Sci*. 2009; 28:123–138.
17. Fan YQ, Ren JY, Onstot W, Pasale J, Tsotsis TT, Egolfopoulos FN. Reactor and technical feasibility aspects of a CO_2 decomposition-based power generation cycle, utilizing a high temperature membrane reactor. *Ind Eng Chem Res*. 2003;42:2618–2626.
18. Arnold M, Wang HH, Feldhoff A. Influence of CO_2 on the oxygen permeation performance and the microstructure of perovskite-type $(Ba_{0.5}Sr_{0.5})(Co_{0.8}Fe_{0.2})O_{3-\delta}$ membranes. *J Membr Sci*. 2007;293:44–52.
19. Yi JX, Feng SJ, Zuo YB, Liu YB, Chen CS. Oxygen permeability and stability of $Sr_{0.95}Co_{0.8}Fe_{0.2}O_{3-\delta}$ in a CO_2 and H_2O-containing atmosphere. *Chem Mater*. 2005;17:5856–5861.
20. Ten Elshof JE, Nguyen NQ, Den Otter MW, Bouwmeester HJM. Oxygen permeation properties of dense $Bi_{1.5}Er_{0.5}O_3$-Ag cermet membranes. *J Electrochem Soc*. 1997;144:4361–4366.
21. Kobayashi K, Tsunoda T. Oxygen permeation and electrical transport properties of 60 vol % $Bi_{1.6}Y_{0.4}O_3$ and 40 vol % Ag composite prepared by the sol-gel method. *Solid State Ionics*. 2004;175:405–408.
22. Kim J, Lin YS. Synthesis and oxygen permeation properties of ceramic-metal dual-phase membranes. *J Membr Sci*. 2000;167:123–133.
23. Kharton VV, Kovalevsky AV, Viskup AP, Shaula AL, Figueiredo FM, Naumovich EN, Marques FMB. Oxygen transport in $Ce_{0.8}Gd_{0.2}O_{2-\delta}$-based composite membranes. *Solid State Ionics*. 2003;160: 247–258.
24. Li W, Tian TF, Shi FY, Wang YS, Chen CS. $Ce_{0.8}Sm_{0.2}O_{2-\delta}$-$La_{0.8}Sr_{0.2}MnO_{3-\delta}$ dual-phase composite hollow fiber membrane for oxygen separation. *Ind Eng Chem Res*. 2009;48:5789–5793.
25. Wang B, Zhan MC, Liu W, Chen CS. Oxygen permeation and stability of $Zr_{0.8}Y_{0.2}O_{0.9}$-$La_{0.8}Sr_{0.2}CrO_{3-\delta}$ dual-phase composite. *J Solid State Electrochem*. 2006;10:625–628.
26. Li QM, Zhu XF, Yang WS. Single-step fabrication of asymmetric dual-phase composite membranes for oxygen separation. *J Membr Sci*. 2008;325:11–15.
27. Zhu XF, Wang HH, Yang WS. Relationship between homogeneity and oxygen permeability of composite membranes. *J Membr Sci*. 2008;309:120–127.
28. Luo HX, Tian BB, Wei YY, Wang HH, Jiang HQ, Caro J. Oxygen permeability and structural stability of a novel tantalum-doped perovskite $BaC_{o0.7}F_{e0.2}T_{a0.1O3-\delta}$. *AIChE J*. 2010;56:604–610.
29. Yi JX, Zuo YB, Liu W, Winnubst L, Chen CS. Oxygen permeation through a $Ce_{0.8}Sm_{0.2}O_{2-\delta}$-$La_{0.8}Sr_{0.2}CrO_{3-\delta}$ dual-phase composite membrane. *J Membr Sci*. 2006;280:849–855.
30. Zhu XF, Cong Y, Yang WS. Effects of synthesis methods on oxygen permeability of $BaCe_{0.15}Fe_{0.85}O_{3-\delta}$ ceramic membranes. *J Membr Sci*. 2006;283:158–163.
31. Feldhoff A, Arnold M, Martynczuk J, Gesing TM, Wang HH. The sol-gel synthesis of perovskites by an EDTA/citrate complexing method involves nanoscale solid state reactions. *Solid State Sci*. 2008;10:689–701.
32. Lane JA, Kilner JA. Oxygen surface exchange on gadolinia doped ceria. *Solid State Ionics*. 2000;136–137:927–932.
33. Yashiro K, Onuma S, Kaimai A, Nigara Y, Kawada T, Mizusaki J, Kawwamura K, Horita T, Yokokawa H. Mass transport properties of $Ce_{0.9}Gd_{0.1}O_{3-\delta}$ at the surface and in the bulk. *Solid State Ionics*. 2002;152–153:469–476.
34. ten Elshof JE, Bouwmeester HJM, Verweij H. Oxygen transport through $La_{1-x}Sr_xFeO_{3-\delta}$ membranes. II. Permeation in air/CO, CO_2 gradients. *Solid State Ionics*. 1996;89:81–92.
35. Kharton VV, Tsipis EV, Naumovich EN, Thursfield A, Patrakeev MV, Kolotygin VA, Waerenborgh JC, Metcalfe IS. Mixed conductivity, oxygen permeability and redox behavior of K_2NiF_4-type $La_2Ni_{0.9}Fe_{0.1}O_{4+\delta}$. *J Solid State Chem*. 2008;181:1425–1433.

Manuscript received July 26, 2010, and revision received Sep. 16, 2010.